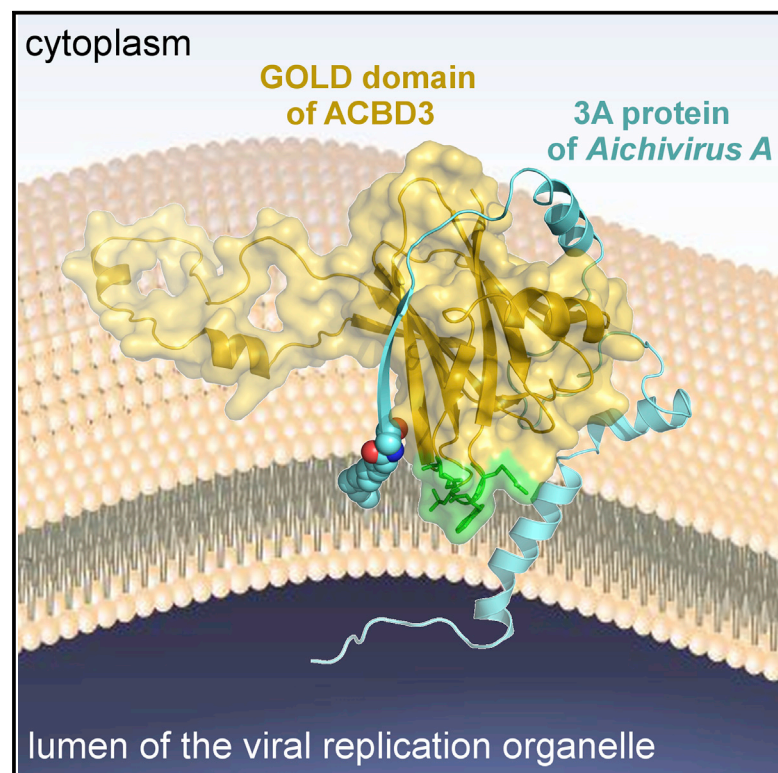


Structure

Kobuviral Non-structural 3A Proteins Act as Molecular Harnesses to Hijack the Host ACBD3 Protein

Graphical Abstract



Authors

Martin Klima, Dominika Chalupska, Bartosz Różycki, ..., Adriana Baumlova, Anna Dubankova, Evzen Boura

Correspondence

klima@uochb.cas.cz (M.K.), boura@uochb.cas.cz (E.B.)

In Brief

Klima et al. report the crystal structure of the ACBD3 GOLD domain in complex with the Aichi virus 3A protein. It reveals that 3A proteins pin down ACBD3 to the target membrane. The efficiency depends on a novel membrane-binding site within the GOLD domain.

Highlights

- Non-structural 3A proteins of the Aichi virus interact with the ACBD3 GOLD domain
- Crystal structures of the GOLD domain and two GOLD:3A complexes are presented
- MD simulations revealed a novel membrane-binding site of the GOLD:3A complex
- Functional studies confirmed the conclusions drawn from the structural analysis

Accession Numbers

5LZ1

5LZ3

5LZ6

Kobuviral Non-structural 3A Proteins Act as Molecular Harnesses to Hijack the Host ACBD3 Protein

Martin Klima,^{1,*} Dominika Chalupska,¹ Bartosz Różycki,² Jana Humpolickova,¹ Lenka Rezabkova,³ Jan Silhan,¹ Adriana Baumlova,¹ Anna Dubankova,¹ and Evzen Boura^{1,4,*}

¹Institute of Organic Chemistry and Biochemistry, Czech Academy of Sciences, 16610 Prague, Czech Republic

²Institute of Physics, Polish Academy of Sciences, 02-668 Warsaw, Poland

³Laboratory of Biomolecular Research, Department of Biology and Chemistry, Paul Scherrer Institute, 5232 Villigen PSI, Switzerland

⁴Lead Contact

*Correspondence: klima@uochb.cas.cz (M.K.), boura@uochb.cas.cz (E.B.)

<http://dx.doi.org/10.1016/j.str.2016.11.021>

SUMMARY

Picornaviruses are small positive-sense single-stranded RNA viruses that include many important human pathogens. Within the host cell, they replicate at specific replication sites called replication organelles. To create this membrane platform, they hijack several host factors including the acyl-CoA-binding domain-containing protein-3 (ACBD3). Here, we present a structural characterization of the molecular complexes formed by the non-structural 3A proteins from two species of the *Kobuvirus* genus of the Picornaviridae family and the 3A-binding domain of the host ACBD3 protein. Specifically, we present a series of crystal structures as well as a molecular dynamics simulation of the 3A:ACBD3 complex at the membrane, which reveals that the viral 3A proteins act as molecular harnesses to enslave the ACBD3 protein leading to its stabilization at target membranes. Our data provide a structural rationale for understanding how these viral-host protein complexes assemble at the atomic level and identify new potential targets for antiviral therapies.

INTRODUCTION

Picornaviruses are small, non-enveloped viruses with icosahedral capsids, utilizing positive-sense single-stranded RNA (+RNA) as their genetic material. Upon infection, the viral genome is translated from a single open reading frame into a polypeptide, which is processed into a variety of precursor and mature proteins including the non-structural protein 3A. This protein is a critical component of the viral replication complex and it associates with the viral replication organelles via its own C-terminal hydrophobic membrane-binding region (Fujita et al., 2007). The major part of the 3A protein, its N-terminal soluble cytoplasmic domain, is mostly unstructured yet functional, as documented for the 3A protein of poliovirus, the prototypical member of the Picornaviridae family (Strauss et al., 2003). The 3A proteins

of various picornaviruses play an important role in the membrane reorganization and inhibition of the host cell endoplasmic reticulum-to-Golgi transport pathways. To achieve this, they recruit several cellular host factors to the viral replication organelles by direct protein-protein interactions. For instance, the 3A protein from the encephalomyocarditis virus (genus *Cardiovirus*) interacts with the host lipid kinase phosphatidylinositol 4-kinase alpha (PI4KA) (Dorobantu et al., 2015a), the 3A proteins from several members of the *Enterovirus* genus (e.g., poliovirus) interact with the host Golgi-specific brefeldin A-resistant guanine nucleotide exchange factor 1 (Wessels et al., 2006), and the 3A proteins from several viruses of both *Enterovirus* and *Kobuvirus* genera (e.g., aichivirus) interact with the host acyl-CoA-binding domain-containing protein-3 (ACBD3) (Greninger et al., 2012; Sasaki et al., 2012).

ACBD3 (also known as GCP60, PAP7, GOCAP1, GOLPH1) is a Golgi-resident protein involved in the maintenance of the Golgi structure and function (Fan et al., 2010). Membrane localization of ACBD3 is mediated by direct interaction with the Golgi integral protein golgin B1/giantin (Sohda et al., 2001). ACBD3 functions as an adaptor protein, a hub for various protein-protein interactions, and hence it participates in a plethora of cellular signaling pathways (Fan et al., 2010). In a tissue- and cell-specific manner, ACBD3 can interact with a number of proteins including the lipid kinase phosphatidylinositol 4-kinase β (PI4KB) to regulate lipid homeostasis (Greninger et al., 2012; Klima et al., 2016; Sasaki et al., 2012). Although the 3A proteins from several picornaviruses can form a stable ternary complex with ACBD3 and PI4KB (Greninger et al., 2012, 2013; Ishikawa-Sasaki et al., 2014; Sasaki et al., 2012), PI4KB can be recruited to the viral replication organelles even in cells depleted of ACBD3 (Dorobantu et al., 2014, 2015b). This implies that some viruses (e.g., rhinovirus-2, coxsackievirus B3) recruit PI4KB independently of ACBD3 and that the 3A:ACBD3 interaction may also serve other purposes besides PI4KB recruitment.

In this study we present the biochemical and structural characterization of two molecular complexes formed by the 3A proteins from two species of the *Kobuvirus* genus (i.e., *Aichivirus A* and *Aichivirus B*) and the 3A-binding Golgi dynamics domain (GOLD) of the host ACBD3 protein. Specifically, we present a series of crystal structures at resolutions in the range of 2.1–3.1 Å of either the unliganded GOLD domain or the GOLD domain in complex

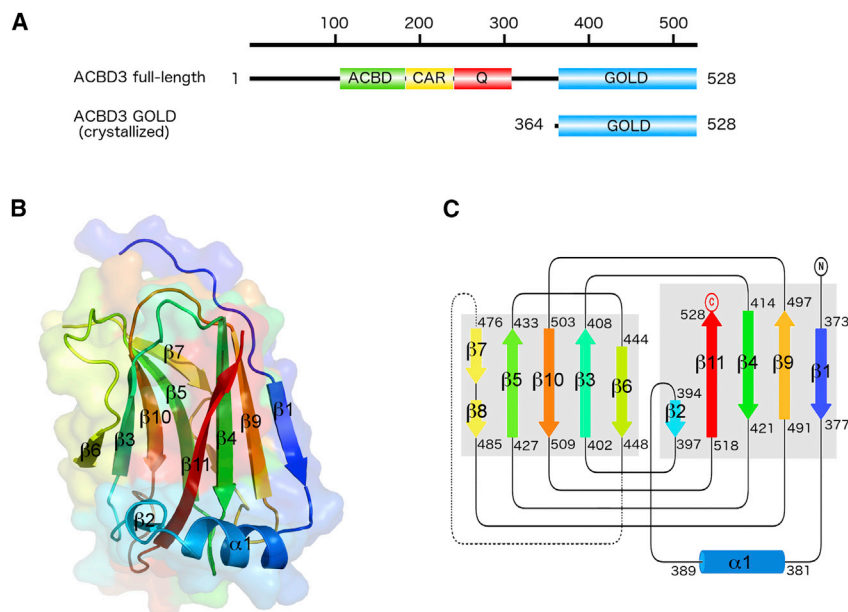


Figure 1. Crystal Structure of the Human ACBD3 GOLD Domain

(A) Schematic representation of the full-length ACBD3 and the construct used for crystallization. ACBD, acyl-CoA-binding domain; CAR, charged amino acids region; Q, glutamine-rich region; GOLD, Golgi dynamics domain.

(B) The overall fold of the ACBD3 GOLD domain. It is composed of one α helix ($\alpha 1$) and 11 β strands (numbered $\beta 1$ - $\beta 11$) forming a distorted jellyroll β barrel-like structure. The protein backbone in cartoon representation as well as its semi-transparent surface is depicted in rainbow colors from blue (N terminus) to red (C terminus).

(C) Topology plot of the ACBD3 GOLD domain.

See also Figure S1.

with these 3A proteins. We show that the 3A proteins, which are mostly intrinsically disordered alone, adopt highly ordered structures when bound to a host factor. To our knowledge, these studies present the first crystal structures of any picornaviral 3A proteins in complex with any host factor. In addition, we show that ACBD3 in complex with the 3A protein is stabilized at target membranes via a previously unknown membrane-binding site. Taken together, our data provide a structural rationale for understanding how these viral-host protein complexes assemble at the atomic level and identify new potential targets for antiviral therapies.

RESULTS

The Crystal Structure of the Human ACBD3 GOLD Domain

ACBD3 has been reported as a host factor for multiple picornaviruses, including several species of the *Enterovirus* and *Kobuvirus* genera (Greninger et al., 2012). ACBD3 is recruited to the viral replication organelles via direct interactions with the viral non-structural 3A proteins. Despite the fact that these 3A proteins share less than 30% identity at the amino acid level, both enteroviral and kobuviral 3A proteins directly interact with the C-terminal domain of ACBD3 known as GOLD (Dorobantu et al., 2014; Greninger et al., 2013; Sasaki et al., 2012). GOLD domains are β -strand-rich domains proposed to mediate diverse protein-protein interactions (Anantharaman and Aravind, 2002). They are present in a variety of proteins with roles in Golgi dynamics and transport of cargo molecules from the endoplasmic reticulum to the Golgi. Within the human proteome GOLD domains have been found in Sec14-like proteins, Emp24-like proteins, and ACBD3.

ACBD3 is a multidomain protein composed of an N-terminal acyl-CoA-binding domain, a PI4KB-binding glutamine-rich domain, and a C-terminal 3A-binding GOLD domain linked by large intrinsically disordered regions that impede crystallization of

the full-length protein (Figure 1A). For the crystallographic analysis of the human ACBD3 GOLD domain we generated a series of N-terminally truncated constructs of ACBD3. The best crystals were obtained with a construct encoding residues 364–528 of ACBD3 (Figure 1A). The crystals diffracted to 2.08 Å and belonged to the tetragonal P4₃2₁2 space group with one molecule per asymmetric unit. The structure was subsequently solved by molecular replacement/single-wavelength anomalous dispersion (MR-SAD) using the GOLD domain of human SEC14L2 as a search model and the anomalous signal from the selenomethionine-containing crystals and refined to R_{free} = 24.74% and R_{work} = 21.81% (Tables 1 and S1). We were able to trace the entire polypeptide chain from E364 to R528 except for one disordered loop between residues S448 and K473. The structure revealed a distorted jellyroll β -barrel-like fold composed of one α helix ($\alpha 1$) and 11 β strands (numbered as $\beta 1$ - $\beta 11$) (Figures 1B and 1C).

Structural comparison of the ACBD3 GOLD domain and its closest structural relative, the GOLD domain of the human SEC14L2 protein, revealed that the ACBD3 GOLD domain contains an additional N-terminal $\alpha 1^{ACBD3}$ helix and $\beta 1^{ACBD3}$ strand, while it lacks the C-terminal $\alpha 2^{SEC14L2}$ helix present in SEC14L2 (Figure S1A). In addition, the ACBD3 GOLD domain contains an intrinsically disordered loop between β strands $\beta 6^{ACBD3}$ and $\beta 7^{ACBD3}$. This segment was predicted (Yang et al., 2014) to contain two short α helices numbered as $\alpha 2^{ACBD3}$ and $\alpha 3^{ACBD3}$ (Figure S1B). Multiple alignment of the ACBD3 GOLD domain orthologs confirmed its conservation from flatworms to mammals with a significantly lower conservation of the intrinsically disordered loop compared with the highly conserved ordered regions of this domain (Figure S1C).

Biochemical Characterization of the Interaction of the ACBD3 GOLD Domain and Kobuviral Non-structural 3A Proteins

In general, picornaviral non-structural 3A proteins are composed of an N-terminal soluble cytoplasmic domain and a C-terminal hydrophobic membrane-binding region that anchors the 3A proteins to the viral replication organelles (Fujita et al., 2007). The 3A proteins of various picornaviruses directly interact via their N-terminal soluble domains with several host proteins in order to

Table 1. Data Collection and Refinement Statistics

Crystal	Native GOLD	SeMet GOLD	GOLD + AiV-A 3A	GOLD + AiV-B 3A
PDB:	5LZ1		5LZ3	5LZ6
Data Collection and Processing				
Space group	P 43 21 2	P 31 2 1	I 2 2 2	P 31 2 1
Cell dimensions				
a, b, c (Å)	56.2, 56.2, 163.9	52.8, 52.8, 130.9	54.1, 81.2, 117.6	55.6, 55.6, 144.3
α, β, γ (°)	90, 90, 90	90, 90, 120	90, 90, 90	90, 90, 120
Diffraction source	BESSY ID 14-1	BESSY ID 14-1	home source	BESSY ID 14-1
Wavelength (Å)	1.2827	0.9798	1.5419	0.9798
Resolution at $I/\sigma(I) = 2$	2.08	2.93	3.11	2.75
Resolution range (Å)	39.75–2.00 (2.07–2.00)	45.75–2.79 (2.89–2.79)	26.36–3.00 (3.11–3.00)	48.18–2.60 (2.69–2.60)
No. of unique reflections	18,582 (1,800)	5,646 (540)	5,185 (504)	8,472 (819)
Mean $I/\sigma(I)$	18.66 (1.43)	21.16 (1.75)	7.90 (1.68)	22.47 (1.24)
Completeness (%)	99.85 (99.45)	99.91 (99.63)	95.26 (96.55)	99.96 (100.00)
Multiplicity	7.7 (7.9)	18.5 (17.5)	4.1 (4.3)	10.4 (10.8)
Structure Solution and Refinement				
R_{work} (%)	21.81 (31.10)		21.84 (30.48)	21.49 (36.31)
R_{free} (%)	24.75 (37.00)		24.81 (37.52)	26.03 (32.89)
CC1/2	0.999 (0.631)		0.981 (0.691)	1.000 (0.454)
CC*	1.000 (0.880)		0.995 (0.904)	1.000 (0.790)
No. of non-H atoms	1,172		1,301	1,279
RMSD				
Bonds (Å)	0.003		0.005	0.003
Angles (°)	0.90		0.77	0.71
Average B factors (Å ²)	50.50		42.80	74.70
Ramachandran favored/outliers (%)	99/0		99/0	97/0

Statistics for data collection and processing, structure solution and refinement of the native and selenomethionine-containing unliganded human ACBD3 GOLD domain as well as the GOLD domain in complex with the 3A protein from *Aichivirus A* and *Aichivirus B*. Numbers in parentheses refer to the highest-resolution shell of the respective dataset. Please see [Tables S1](#) and [S2](#) for more details. RMSD, root-mean-square deviation.

recruit them to viral replication sites. Here, we focused on biochemical characterization of the complexes composed of the ACBD3 GOLD domain and non-structural 3A proteins from the species of the *Kobuvirus* genus, hereafter referred to as GOLD:3A complexes.

Currently, the *Kobuvirus* genus consists of three species named *Aichivirus A* (AiV-A, also known as Aichi virus-1 or human Aichi virus), *Aichivirus B* (AiV-B, Aichi virus-2 or bovine kobuvirus), and *Aichivirus C* (AiV-C, Aichi virus-3 or porcine kobuvirus) (Reuter et al., 2011). We generated recombinant 3A proteins from all three of these viruses truncated of their C-terminal hydrophobic regions (Figure 2A) and used them to verify the direct GOLD:3A interaction in our model system, which lacks any potential eukaryotic proteins that can mediate an indirect interaction. Using an in vitro binding assay, we found that the ACBD3 full-length protein as well as the ACBD3 GOLD domain specifically co-purified with the NiNTA-immobilized N-terminally His₆GB1 (G protein B1 domain)-tagged 3A proteins from all three kobuviruses, suggesting a direct interaction and confirming the localization of the 3A-binding region to the GOLD domain of ACBD3 (Figure 2B).

Next, we performed analytical ultracentrifugation to determine the stoichiometry of the recombinant GOLD:3A protein complex. The sedimentation coefficients of the GOLD domain and the

GOLD:3A complex were determined as 1.9 S and 2.1 S, corresponding to the molecular weights of approximately 20 and 24 kDa, respectively (Figure 2C). This result suggests that both proteins are monomeric and the stoichiometry of the GOLD:3A protein complex is 1:1. Finally, we determined the strength of the GOLD:3A interaction using two independent approaches: surface plasmon resonance (SPR, Figure 2D) and microscale thermophoresis (MST, see Figure 4 for more detail). The SPR assay showed an interaction with a dissociation constant in the low-micromolar range with slightly higher affinity of the ACBD3 GOLD domain to the 3A proteins of *Aichivirus B* ($K_D = 8.0 \pm 1.2 \mu\text{M}$) and *Aichivirus C* ($K_D = 3.8 \pm 0.7 \mu\text{M}$) compared with the affinity to the 3A protein from *Aichivirus A* ($K_D = 19 \pm 3 \mu\text{M}$, Figure 2D). In summary, ACBD3 and kobuviral 3A proteins interact directly through the GOLD domain of ACBD3 and the N-terminal domain of the 3A proteins with a 1:1 stoichiometry and with a dissociation constant within the micromolar range.

Crystal Structures of the ACBD3 GOLD Domain in Complex with the Non-structural 3A Proteins from *Aichivirus A* and *Aichivirus B*

For crystallographic analysis of the GOLD:3A complexes, we co-crystallized the respective recombinant 3A proteins truncated of

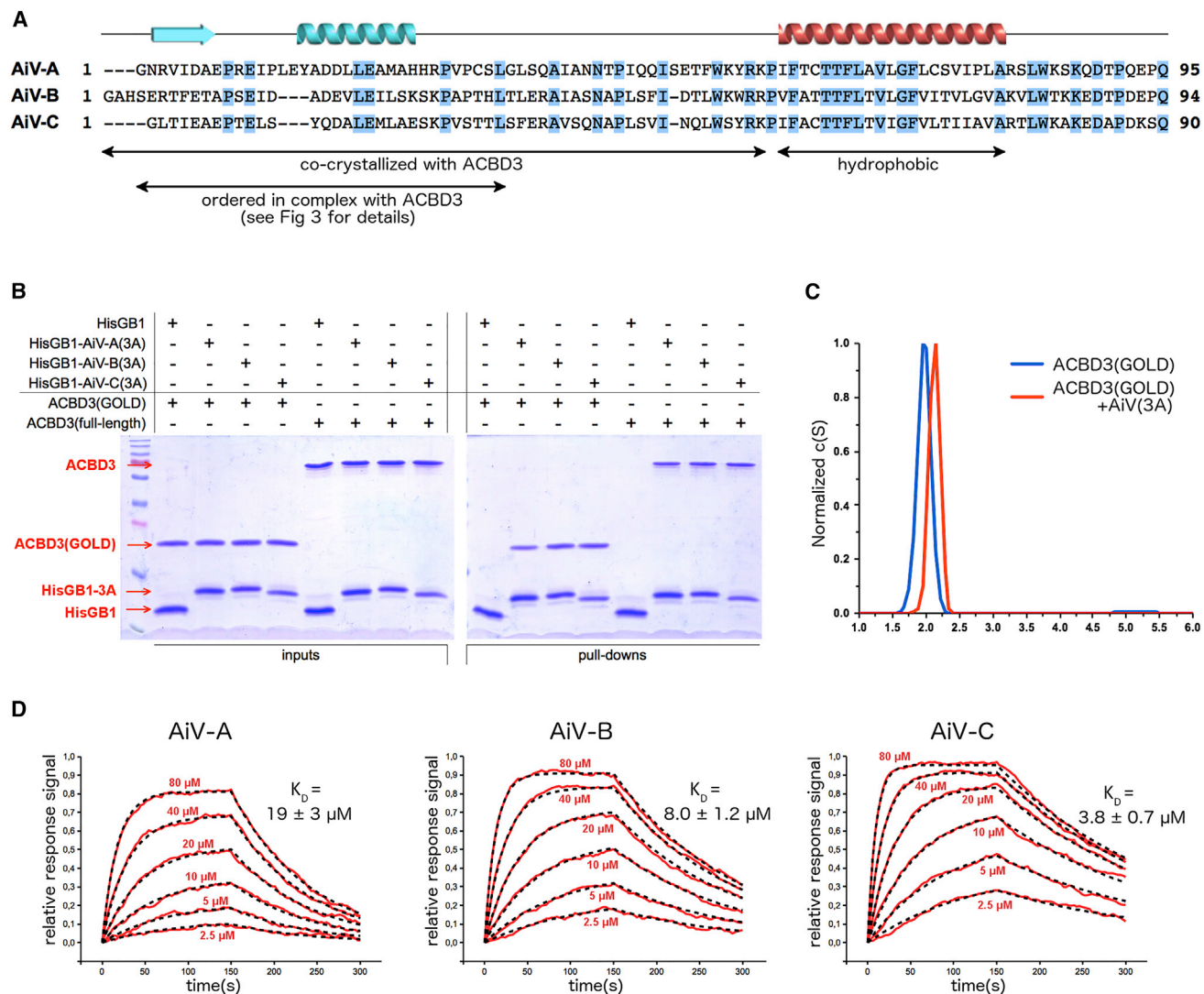


Figure 2. Biochemical Characterization of the GOLD:3A Complexes

(A) Multiple alignment of the 3A proteins from viruses of the *Kobovirus* genus. Sequences were obtained from GenBank and aligned using the ClustalX algorithm as follows: the 3A protein from *Aichivirus A* (also known as human Aichi virus, GenBank: NP_047200_1), *Aichivirus B* (also known as bovine kobovirus, GenBank: NP_740257_1), *Aichivirus C* (also known as porcine kobovirus, GenBank: YP_002456506_1). Blue areas represent conserved amino acids; the numbers indicate amino acids positions. The secondary structures present in the crystal structure (colored in aquamarine) as well as the proposed transmembrane α helix (colored in red) are indicated above the sequences.

(B) In vitro pull-down assays with NiNTA-immobilized N-terminally His₆GB1-tagged koboviral 3A proteins and untagged full-length ACBD3 or the ACBD3 GOLD domain. The inputs and bound proteins were analyzed on SDS gels stained with Coomassie blue.

(C) Analytical ultracentrifugation analysis of the unliganded ACBD3 GOLD domain and the GOLD domain in complex with the AiV-A 3A protein at the concentration of 50 μ M.

(D) SPR analysis of the interaction of the ACBD3 GOLD domain and koboviral 3A proteins. Sensograms for six concentrations of the 3A proteins are shown. Changes in the relative response signal and the fitting curves are displayed as solid red lines and black dashed lines, respectively. The dissociation constants are presented as mean values \pm SEM based on three independent experiments.

their C-terminal hydrophobic regions with the ACBD3 GOLD domain (Figure 2A). All three species of the GOLD:3A complexes formed crystals; however, only the GOLD:3A crystals with the 3A proteins from *Aichivirus A* and *Aichivirus B* (hereafter referred to as GOLD:3A/AiV-A and GOLD:3A/AiV-B crystals, respectively) diffracted to a resolution suitable for further structure determination. The GOLD:3A crystals with the 3A protein from *Aichivirus C* diffracted poorly due to their extremely small size even after

extensive optimization. The GOLD:3A/AiV-A crystals diffracted to 3.11 \AA and belonged to the orthorhombic I222 space group, while the GOLD:3A/AiV-B crystals diffracted to 2.75 \AA and belonged to the trigonal P3₁21 space group, with one GOLD:3A complex per asymmetric unit for both crystal species. Both structures were subsequently solved by MR using the previously obtained structure of the unliganded ACBD3 GOLD domain as a search model; the GOLD:3A/AiV-A structure was further refined

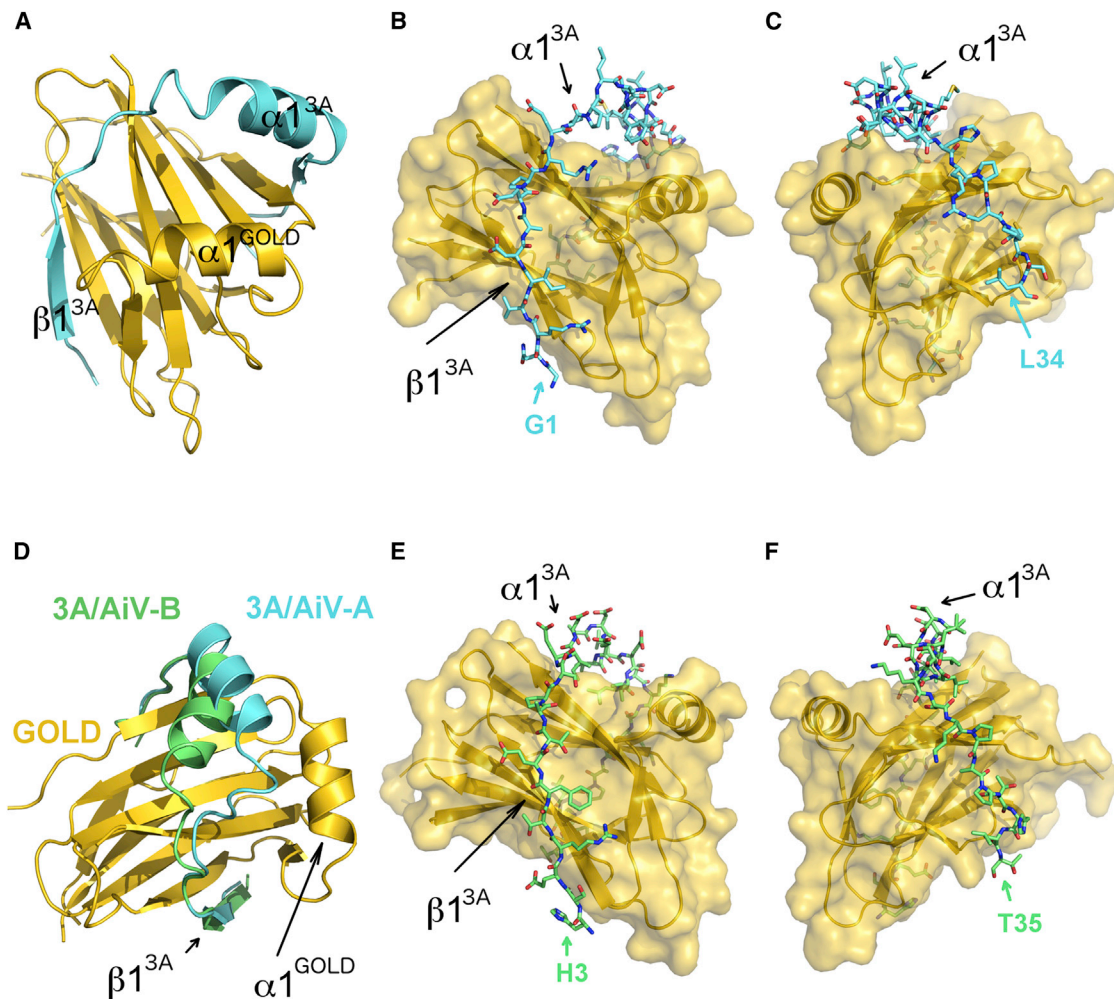


Figure 3. Structural Characterization of the GOLD:3A Complexes

- (A) The overall fold of the GOLD:3A/AiV-A complex. The protein backbone is shown in cartoon representation. The ACBD3 GOLD domain is depicted in gold, the viral 3A protein in aquamarine.
- (B) Detailed view of the GOLD:3A/AiV-A complex. The protein backbone in cartoon representation as well as the semi-transparent surface of the ACBD3 GOLD domain is depicted in gold. The viral 3A protein is shown in stick representation and colored according to elements—carbons are colored in aquamarine, oxygens in red, nitrogens in blue, sulfurs in yellow.
- (C) The view from (B) rotated by 220°.
- (D) Superposition of the GOLD:3A/AiV-A and GOLD:3A/AiV-B complexes. The protein backbone is shown in cartoon representation. The ACBD3 GOLD domain is depicted in gold, the AiV-A 3A protein in aquamarine, the AiV-B 3A protein in green.
- (E) Detailed view of the GOLD:3A/AiV-B complex depicted as in (C) with the viral 3A protein carbons colored in green.
- (F) The view from (E) rotated by 220°.

to $R_{\text{free}} = 24.81\%$ and $R_{\text{work}} = 21.84\%$, while the GOLD:3A/AiV-B structure was refined to $R_{\text{free}} = 26.03\%$ and $R_{\text{work}} = 21.49\%$ (Tables 1 and S2).

In the GOLD:3A/AiV-A structure we were able to trace the entire polypeptide chain of the 3A protein from G1^{3A} to L34^{3A} (Figures 3A–3C). The structure revealed that the viral 3A protein adopts a highly ordered structured conformation when it is bound to the host ACBD3 protein. It contains an N-terminal β strand R3^{3A}-A7^{3A} ($\beta 1^{3A}$), a central α helix L14^{3A}-H26^{3A} ($\alpha 1^{3A}$), and a C-terminally located strand H27^{3A}-L34^{3A}. The $\beta 1^{3A}$ strand of the 3A protein is tightly bound to the $\beta 3^{\text{GOLD}}$ strand of ACBD3 at a similar position as the $\beta 6^{\text{GOLD}}$ strand in the structure of the unliganded GOLD domain. Interestingly, the $\beta 3^{\text{GOLD}}$

and $\beta 6^{\text{GOLD}}$ strands in the structure of the unliganded GOLD domain are antiparallel, while the $\beta 1^{3A}$ and $\beta 3^{\text{GOLD}}$ strands in the GOLD:3A/AiV-A structure are parallel. The segment forming the $\beta 6^{\text{GOLD}}$ strand in the structure of the unliganded GOLD domain becomes unstructured in the GOLD:3A/AiV-A complex, expanding the intrinsically disordered loop S448-K473 in the structure of the unliganded GOLD domain to T436-K473 in the GOLD:3A/AiV-A complex. The replacement of the $\beta 6^{\text{GOLD}}$ strand in the structure of the unliganded GOLD domain by the $\beta 1^{3A}$ strands in the GOLD:3A/AiV-A structure mechanically reflects the high affinity of the $\beta 1^{3A}$ strand of the 3A protein to the $\beta 3^{\text{GOLD}}$ strand of ACBD3 as discussed later. The central $\alpha 1^{3A}$ helix of the 3A protein is rather flexible and its conformation within the crystal

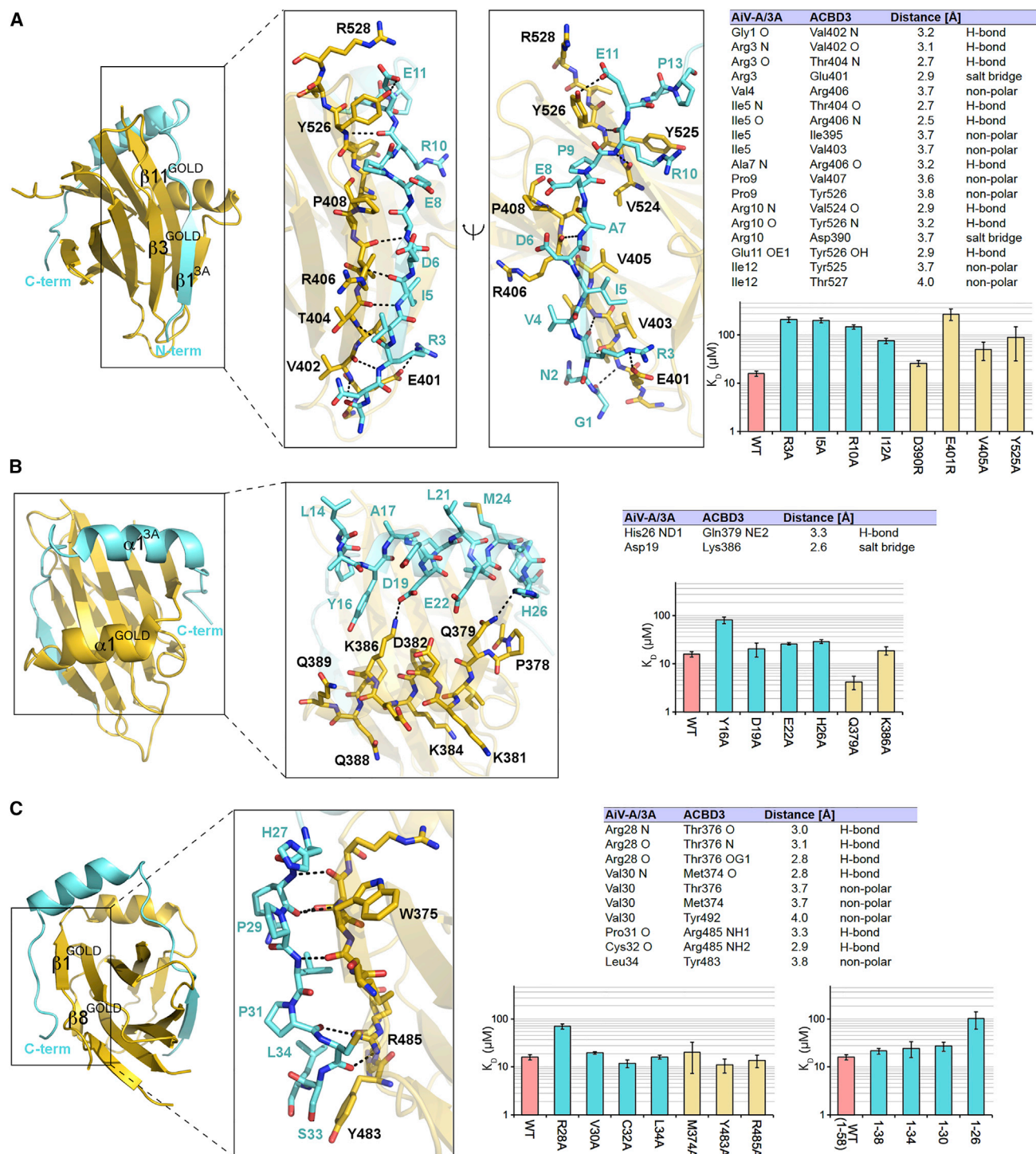


Figure 4. Detailed View of the Interface of the GOLD:3A/AiV-A Complex

Detailed view of the interface between the GOLD domain and the 3A protein residues G1-P13 (A), P13-H26 (B), and H27-L34 (C), respectively.

Left panel, the overall and detailed view of the indicated segments is shown. The protein backbones are shown in semi-transparent cartoon representations; the ACBD3 GOLD domain is depicted in gold, the AiV-A 3A protein in aquamarine. In the detailed view, the amino acid residues from the indicated segments are shown in stick representation and colored according to elements—oxygen atoms are colored in red, nitrogen atoms in blue, sulfur atoms in yellow, carbon atoms are colored according to the protein assignment. Hydrogen bonds are shown as dotted black lines; hydrogen atoms are not shown.

(legend continued on next page)

is partially fixed by symmetric hydrophobic crystal contacts with molecules from other asymmetric units, mediated by residues L14^{3A}, A17^{3A}, L20^{3A}, L21^{3A}, and M24^{3A}. The C-terminal strand of the 3A protein interacts with several residues from the $\beta 1^{\text{GOLD}}$ and $\beta 8^{\text{GOLD}}$ strands of ACBD3.

Despite the fact that the primary sequence homology of the soluble domains of the 3A proteins of *Aichivirus A* and *Aichivirus B* reaches only 36% (Figure 2A), the overall structure of the GOLD:3A/AiV-B complex is highly similar to that of the GOLD:3A/AiV-A complex (Figures 3D–3F). The superposition of these complexes revealed only a minor change in the position of the central $\alpha 1^{3A}$ helix of the 3A protein confirming its flexibility (Figure 3D).

Analysis of the Interface between the ACBD3 GOLD Domain and the Non-structural AiV-A 3A Protein

To corroborate the structural data and to analyze the interface between the ACBD3 GOLD domain and the viral 3A proteins, we introduced a number of point mutations into both proteins and validated their effect on complex formation and the strength of the interaction using the MST assay. The GOLD:3A interaction is mediated through multiple hydrogen bonds, hydrophobic interactions, and salt bridges (Figure 4). The intermediary part of the AiV-A 3A protein present in the crystal structure is composed of four segments as follows: N-terminal β strand G1-E8, loop P9-P13, middle helix L14-H26, and C-terminal strand H27-L34. The N-terminal strand G1-E8 and the loop P9-P13 form the segment with the highest affinity to the GOLD domain (Figure 4A). The most prominent interactions between this segment and the GOLD domain are represented by the non-polar interaction of the I5^{3A} residue with a hydrophobic pocket formed by the V403^{GOLD}, V405^{GOLD}, and I395^{GOLD} residues, and by the salt bridges between the R3^{3A} and E401^{GOLD}, and between the R10^{3A} and D390^{GOLD} residues. The most dramatic reduction of the GOLD:3A affinity was caused by the R3A^{3A}, I5A^{3A}, and E401R^{GOLD} mutations (Figure 4A). The V403A^{GOLD} and I395A^{GOLD} mutants expressed poorly in bacteria, implying probable folding defects, and thus were excluded from further analysis.

The interaction of the central helix of the 3A protein L14-H26 with the GOLD domain is significantly weaker. Its conformation within the crystal is fixed by symmetric crystal contacts with molecules from other asymmetric units. Moreover, its position within the GOLD:3A/AiV-B structure is shifted probably due to different crystal contacts. Two possible interactions of this segment within the GOLD:3A/AiV-A crystal structure are present: a hydrogen bond between the H26^{3A} and Q379^{GOLD} residues, and a salt bridge between the D19^{3A} and K386^{GOLD} residues (Figure 4B). However, mutagenesis of these residues led either to a minor reduction of the GOLD:3A affinity or, in case of the Q379A^{GOLD} mutation, even strengthened this interaction, confirming the flexibility of this segment in solution.

The C-terminal segment of the 3A protein H27-L34 forms several hydrogen bonds and non-polar interactions with the $\beta 1^{\text{GOLD}}$ and $\beta 8^{\text{GOLD}}$ strands of the GOLD domain including the R485^{GOLD} residue. Surprisingly, mutation of this R485^{GOLD} residue did not cause an expected reduction of the GOLD:3A affinity (Figure 4C). Moreover, neither deletion of the P31-L34 segment of the 3A protein nor mutagenesis of the V30^{3A}, C32^{3A}, and L34^{3A} residues affected the interaction. On the other hand, further deletion of the H27-V30 segment of the 3A protein as well as the R28A^{3A} mutation strongly inhibited the interaction. These data suggest that the position of the P31-L34 segment within the GOLD:3A crystal structure, including the hydrogen bonds formed by the R485^{GOLD} residue and the main chain oxygens of the P31^{3A} and C32^{3A} residues, does not contribute to the GOLD:3A affinity in solution. Rather, the 3A protein is anchored to the GOLD domain in this region through the H27-V30 segment forming the β -sheet-like hydrogen bonds with the $\beta 1^{\text{GOLD}}$ strand of the GOLD domain.

In summary, the 3A protein is anchored within the GOLD:3A complex to the GOLD domain through its N- and C-terminal strands, with a partially flexible central helix in between. The most important residues of the AiV-A 3A protein for the GOLD:3A interaction are represented by the R3^{3A} and I5^{3A} residues. The interface between the ACBD3 GOLD domain and the kobuviral 3A proteins is highly conserved between *Aichivirus A* and *Aichivirus B* including the most important residues (Figure S2). The R3^{3A/AiV-A} residue is conserved as R6^{3A/AiV-B}, while the I5^{3A/AiV-A} residue is replaced by F8^{3A/AiV-B} in the GOLD:3A/AiV-B structure where it binds to the same hydrophobic pocket as I5^{3A/AiV-A} formed by the V403^{GOLD}, V405^{GOLD}, and I395^{GOLD} residues (Figure S2A).

Analysis of the Membrane-Binding Mode of the GOLD:3A Protein Complex Revealed a Novel Membrane-Binding Site of ACBD3

Within the cells neither ACBD3 nor the viral 3A proteins are present freely in the cytoplasm, rather they are associated with membranes. 3A proteins from all picornaviruses including kobuviruses contain C-terminal hydrophobic membrane-binding regions that anchor the 3A proteins to the viral replication organelles (Fujita et al., 2007). In addition, the N-terminal glycines of the 3A proteins of *Aichivirus A* and *Aichivirus B* are myristoylated despite lacking a canonical myristoylation motif (Greninger et al., 2012). This posttranslational modification of the 3A proteins is very unusual among picornaviruses and, outside kobuviruses, they have been described only in human salivirus (also known as klassevirus) (Greninger et al., 2012).

To gain more insight into the membrane-binding mode(s) of the GOLD:3A protein complex we performed an all-atom molecular dynamics (MD) simulation of the GOLD:3A complex at the surface of the lipid bilayer (see Supplemental Experimental Procedures for details). The atomic coordinates of the core of the

Upper right panel, hydrogen bonds, non-polar interactions, and salt bridges between the GOLD domain and the AiV-A 3A protein are listed. The distance cutoff used for hydrogen bonds is 3.4 Å, for non-polar interactions and salt bridges 4.0 Å. The distances between the indicated residues involved in the non-polar interactions and salt bridges correspond to the closest atom pairs.

Lower right panel, MST analysis of the interactions between the ACBD3 GOLD domain and the AiV-A 3A protein (and their mutants) is shown. Bar graph presents the mean values of the dissociation constants on the logarithmic scale; error bars are SEM based on three independent experiments.

See also Figure S2.

GOLD:3A complex were taken from the present crystal structure, then the missing segments (particularly the GOLD domain residues T436-K473 and the 3A protein residues G35-K58) were modeled, as were the N-terminal myristoyl moiety and the C-terminal transmembrane domain of the 3A protein. The MD simulations uncovered a previously unknown membrane-binding site of the GOLD domain formed by amino acid residues R399, L514, W515, and R516. The hydrophobic residues L514 and W515 are inserted into the lipid bilayer, while the basic residues R399 and R516 interact with phosphorylated lipid head groups (Figure 5A, Movie S1).

To experimentally verify our model, we generated a recombinant GOLD domain with L514 and W515 residues mutated to alanines (hereafter referred to as LW mutant). Under membrane-free conditions (Figure 5B), both wild-type GOLD domain and the LW mutant interact with the NiNTA-immobilized N-terminally His₆GB1-tagged 3A protein in an in vitro binding assay (Figure 5C). The dissociation constants of both interactions were determined in solution using MST and were found to be in a similar range ($K_D = 16 \pm 2 \mu\text{M}$ for the wild-type GOLD domain and $34 \pm 4 \mu\text{M}$ for the LW mutant). The difference is attributable to the local conformational changes associated with the vicinity of the LW mutations to the site where the $\beta 1^{3A}$ strand of the 3A protein is bound to the $\beta 3^{\text{GOLD}}$ strand of the GOLD domain (Figure 5D).

To resemble the in vivo situation with the membrane-bound 3A protein, we established an in vitro membrane recruitment system using biomimetic artificial membranes containing the Ni²⁺-binding DGS-NTA lipid and both N- and C-terminally His₆-tagged 3A protein (His₆-3A-His₆). The His₆-tags in this system mimic the natural attachment of the 3A protein to the membrane via both the N-terminal myristoyl moiety and the C-terminal transmembrane domain (Figure 5E). In agreement with our MD simulations studies, the fluorescently labeled His₆-3A-His₆ protein was able to efficiently recruit the wild-type GOLD domain, but not the LW mutant, to membranes of giant unilamellar vesicles (Figure 5F). The dissociation constant of the GOLD:3A interaction in the presence of a lipid membrane was determined using fluorescence cross-correlation spectroscopy (Schwille et al., 1997). The ratio of the cross-correlation amplitude and the amplitude of the EGFP channel served as a measure of binding of the EGFP-labeled GOLD domain to the large unilamellar vesicles decorated with the His₆-3A-His₆ protein. The dependence of the amplitude ratio on the 3A concentration provided $K_D = 1.9 \pm 0.3 \mu\text{M}$ for the wild-type GOLD domain and a technically undetectable $K_D \gg 20 \mu\text{M}$ for the LW mutant (Figure 5G). The presence of the membrane stabilizes the interaction of the 3A protein with the wild-type GOLD domain, but not with the LW mutant, confirming the presence of the physiologically relevant membrane-binding site within the GOLD domain.

DISCUSSION

Picornaviruses are small, non-enveloped viruses utilizing +RNA as their genetic material. Compared with other +RNA viruses, their genome is very small, ranging between 7.1 and 8.9 kb in length, yet it contains the genetic information sufficient (within the host environment) for all steps of the virus life cycle including entry, viral genome expression, virion assembly, and release.

These viruses have to rely on the host cell and evolved mechanisms to hijack multiple host factors. In this study, we present the structural determinants of a protein-protein interaction that allows picornaviruses to hijack a 60 kDa host factor via no more than 40 amino acid residues of their small non-structural protein, and to acquire the ability to manipulate the host cell endoplasmic reticulum-to-Golgi transport steps and to optimize the lipid composition of the membranes for viral replication.

Aichivirus A (AiV-A) is a human pathogen from the *Kobuvirus* genus of the *Picornaviridae* family (Reuter et al., 2011). AiV-A was identified in environmental screening studies with higher frequency and greater abundance than other human enteric viruses; worldwide, 80%–95% of adults have developed antibodies against the virus. AiV-A infections are associated with diarrhea, abdominal pain, nausea, vomiting, and fever. Although AiV-A infections are often non-symptomatic, they can cause severe gastroenteritis and deaths in children below the age of 5 years, especially in developing countries. There is no available vaccine or effective antiviral treatment. Recently, the structure of AiV-A virions was determined independently using protein crystallography (Sabin et al., 2016) and cryoelectron microscopy (Zhu et al., 2016). However, the non-structural proteins of AiV-A, including the 3A protein, remained structurally uncharacterized. To our knowledge, none of the picornaviral 3A proteins have been characterized structurally in complex with any host factor, probably because of their intrinsically disordered nature and proteolytic instability. The only structural information about a picornaviral 3A protein comes from the solution nuclear magnetic resonance structure of the N-terminal cytoplasmic domain of the 3A protein of poliovirus (Strauss et al., 2003).

Here, we present the biochemical and structural characterization of the 3A proteins from two species of the *Kobuvirus* genus, i.e., *Aichivirus A* and *Aichivirus B* (AiV-B, also known as bovine kobuvirus). We hypothesized that the picornaviral 3A proteins become structured upon binding the host factor. We optimized the domain boundaries of the 3A proteins from AiV-A and AiV-B as well as their binding partner, the human ACBD3 protein, until high-quality crystals were obtained. We report the first crystal structures of a picornaviral non-structural 3A protein in complex with a host factor, and we show that the 3A proteins, which are mostly intrinsically disordered alone, can adopt highly ordered structured conformations when bound to a host factor, such as ACBD3. The 3A proteins from both AiV-A and AiV-B are N-terminally myristoylated and have C-terminal transmembrane helices (both these motives are missing in our structure as they impede crystallization); the intermediary parts of the 3A proteins are almost entirely wrapped around the GOLD domain of ACBD3. We suggest that the 3A proteins clamp down the GOLD domain of the ACBD3 protein to stabilize it at target membranes.

The intermediary part of the AiV-A 3A protein is composed of an N-terminal β strand G1-E8, loop P9-P13, middle helix L14-H26, and a C-terminal strand H27-L34. We performed a mutagenesis analysis and discovered that both the N-terminal β strand and the C-terminal strand of the 3A protein are important for the GOLD:3A protein complex formation, while the interaction of the central helix of the 3A protein with the GOLD domain is not significant. The AiV-B 3A protein exhibits similar contacts with the GOLD domain as does the AiV-A 3A protein within both its N- and C-terminal strands; however, the position of the central

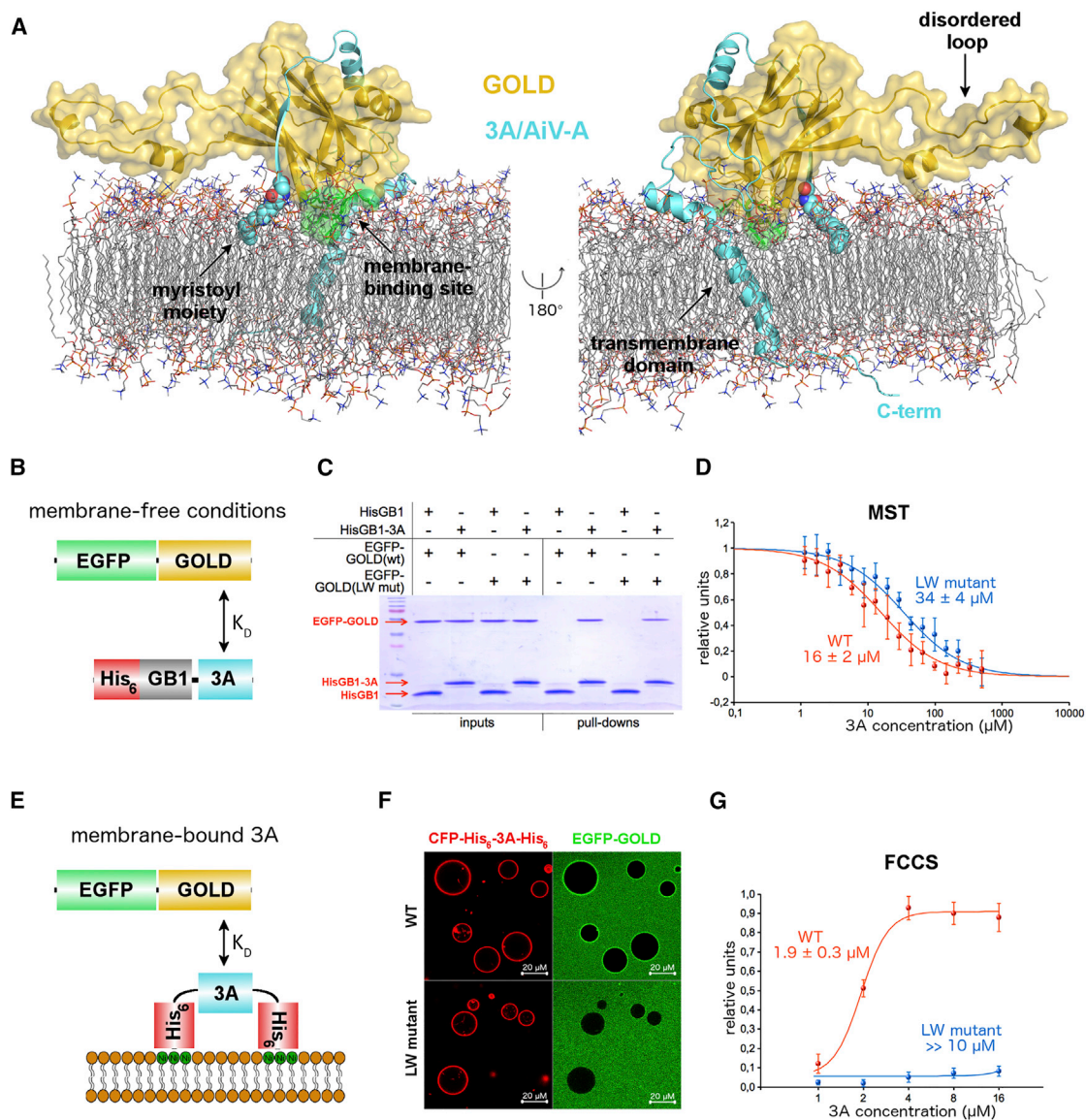


Figure 5. Membrane-Binding Model of the GOLD:3A/AiV-A Complex

(A) Molecular dynamics simulation-based model of the GOLD:3A/AiV-A complex on the lipid bilayer. The viral 3A protein is colored in aquamarine and shown in cartoon representation except for the myristoylated G1 residue which is shown in spheres representation and colored according to elements—carbons are colored in aquamarine, oxygens in red, nitrogen in blue. The ACBD3 GOLD domain is shown in cartoon representation with semi-transparent surface and colored in gold except for the membrane-binding site composed of R399, L514, W515, and R516, which is colored in green. Please see [Movie S1](#) for a 20 ns trajectory of this complex on the lipid bilayer.

(B) Schematic representation of the constructs used for experiments under membrane-free conditions. 3A, N-terminal soluble domain of the AiV-A 3A protein; EGFP, enhanced GFP; GB1, G protein B1 domain (a solubility tag); GOLD, Golgi dynamics domain of ACBD3; K_D , dissociation constant.

(C) In vitro pull-down assays with the NiNTA-immobilized N-terminally His₆GB1-tagged AiV-A 3A protein and the untagged EGFP-fused ACBD3 GOLD domain (wild-type or LW mutant as indicated). The inputs and bound proteins were analyzed on SDS gels stained with Coomassie blue.

(D) MST analysis of the interaction of the AiV-A 3A protein and the EGFP-fused ACBD3 GOLD domain. Plotting of the change in thermophoresis and concomitant fitting curves for the wild-type GOLD domain (depicted in red) compared with the LW mutant (depicted in blue) are shown. Data are presented as mean values \pm SEM based on three independent experiments.

(E) Schematic representation of the constructs used for experiments with the membrane-bound 3A protein. 3A, N-terminal soluble domain of the AiV-A 3A protein; EGFP, enhanced GFP; GOLD, Golgi dynamics domain of ACBD3; K_D , dissociation constant.

(F) GUVs recruitment assay. GUVs were decorated with the CFP-fused AiV-A 3A protein and then mixed with the EGFP-fused ACBD3 GOLD domain (wild-type or LW mutant as indicated). A significant signal of the membrane-bound wild-type GOLD domain (upper panel), but not LW mutant (lower panel), was detected on the surface of GUVs.

(G) Fluorescence cross-correlation spectroscopy (FCCS) analysis of the interaction of the membrane-bound AiV-A 3A protein and the EGFP-fused ACBD3 GOLD domain (wild-type or LW mutant as indicated). The dependence of the ratio of the cross-correlation amplitude and the amplitude of the EGFP channel on the 3A protein concentration is shown. Data are presented as mean values \pm SEM based on three independent experiments.

helix of the AiV-B 3A protein is shifted, probably due to different crystal contacts (resulting in crystallization in a different space group compared with AiV-A 3A). Interestingly, this central helix is the only segment of the N-terminal soluble cytoplasmic domain of the 3A protein which is conserved within the primary sequences among various species of the *Picornaviridae* family regardless of the fact of whether these viruses hijack ACBD3 or not (this sequence often contains a $\Phi\Phi$ BDLL motif, where Φ stands for a hydrophobic residue, B stands for asparagine or aspartic acid). It is strongly amphipathic, it is responsible for the dimerization of the 3A protein from poliovirus (Strauss et al., 2003), but has no biological function assigned yet. Thus, it is possible that through the ACBD3:3A interaction ACBD3 forms a scaffold for this central helix of the 3A protein, which might serve for an unknown protein-protein interaction in order to hijack another unknown host factor.

Under physiological conditions, ACBD3 is localized on the membranes of the Golgi apparatus via a direct protein-protein interaction with a Golgi integral protein golgin B1/giantin (Sohda et al., 2001), which contains a C-terminal membrane-anchoring domain. The ACBD3:giantin interaction was mapped to a region within the GOLD domain of ACBD3 that overlaps with the region essential for the ACBD3:3A interaction, yielding a mutual exclusive interaction either with giantin or the viral 3A protein (Sasaki et al., 2012). In this work, we describe a novel membrane-binding site of ACBD3 which stabilizes the ACBD3:3A complex on the membrane. Although this membrane-binding site of ACBD3 is too weak to capture ACBD3 on the membrane by itself, it is possible that it stabilizes the ACBD3:giantin complex on the membrane under physiological conditions in a similar way as it does with the ACBD3:3A complex upon viral infection.

Upon infection, the AiV-A 3A protein is able to outcompete ACBD3 from the ACBD3:giantin complex on the Golgi membranes and relocate ACBD3 to the place where the viral 3A protein is present (Sasaki et al., 2012), i.e., to the viral replication organelles. The membranes of these organelles have an unusual lipid composition with a high content of phosphatidylinositol 4-phosphate (PI4P) and cholesterol within the cytoplasmic leaflet of the membrane. During the past decade, PI4P has been shown to be an essential minor lipid for replication of many species of +RNA viruses from various genera (Hsu et al., 2010). Among picornaviruses, so far only the encephalomyocarditis virus (genus *Cardiovirus*) was reported to hijack a PI4K by a direct interaction between a viral protein and the host kinase, in this case between the viral 3A protein and the host PI4KA (Dorobantu et al., 2015a). On the contrary, in case of the *Kobuvirus* genus no viral proteins have been found to recruit any of the PI4Ks to the sites of viral replication by a direct interaction. Nevertheless, the AiV-A 3A protein was shown to form a ternary 3A:ACBD3:PI4KB complex through two independent 3A:ACBD3 and ACBD3:PI4KB binary protein-protein interactions (Greninger et al., 2012; Sasaki et al., 2012). The structural determinants of the ACBD3:PI4KB interaction were recently described (Klima et al., 2016), while the structural details of the 3A:ACBD3 complex are described in this work. Genetic inhibition of either ACBD3 or PI4KB reduces AiV-A replication (Ishikawa-Sasaki et al., 2014). Thus, disruption of the 3A:ACBD3:PI4KB complex may represent a novel target for therapeutic intervention without the side effects that can occur during PI4KB inhibition.

Notably, several picornaviruses from the *Enterovirus* genus (e.g., rhinovirus-2, coxsackievirus B3) hijack ACBD3 through the 3A:ACBD3 interaction and even are capable of forming the ternary 3A:ACBD3:PI4KB complex (Greninger et al., 2012); however, PI4KB can be recruited to the viral replication organelles of these viruses even when the cells are depleted of ACBD3 (Dorobantu et al., 2014, 2015b). This implies that these viruses recruit PI4KB to the viral replication sites independently of ACBD3 through a yet to be determined mechanism, and that the 3A:ACBD3 interaction serves also other purposes besides PI4KB recruitment. ACBD3 is involved in the maintenance of the Golgi structure and function including vesicular transport between the endoplasmic reticulum and Golgi (Fan et al., 2010). It is known that some picornaviruses can manipulate the host intracellular transport systems in order to limit the secretion of antiviral cytokines such as interleukin-6 (IL-6), IL-8, and interferon beta (IFN- β) (Dodd et al., 2001), and even to reduce the major histocompatibility complex class I-dependent antigen presentation of the viral peptides (Deitz et al., 2000). These picornaviral activities are also mediated by the 3A protein, nevertheless, whether and to what extent they are dependent on the 3A:ACBD3 interaction are questions to be further investigated.

In summary, we present the first crystal structure of a picornaviral non-structural 3A protein in complex with a cellular host factor, namely ACBD3. Our findings provide structural insights in the process of how these viruses hijack the ACBD3:PI4KB protein complex by elegantly pinning down the ACBD3 GOLD domain to the surface of a lipid bilayer. These studies could provide a structural template for strategies to interrupt the association between the two proteins as a possible approach to combat infections caused by this group of viral pathogens.

EXPERIMENTAL PROCEDURES

Plasmid Construction, Protein Expression, and Purification

Full-length human ACBD3 and kobuviral 3A proteins and their deletion mutants were cloned into pRSFD vector (Novagen) with an N-terminal 6xHis tag followed by a GB1 solubility tag and a tobacco etch virus (TEV) protease cleavage site using restriction cloning. For expression of the EGFP-fused proteins the appropriate mutants were cloned into pHis2 vector with an N-terminal 6xHis tag followed by the TEV protease cleavage site and the EGFP coding region. The proteins were expressed and purified using standard methods as described in detail in the Supplemental Information. Purified proteins were concentrated to 1–10 mg/mL, flash frozen in the liquid nitrogen, and stored at -80°C until needed.

Crystallization and Crystallographic Analysis

The crystallographic datasets were collected at the synchrotron BESSY II (MX14.1 and MX14.3 beamlines) at Helmholtz-Zentrum Berlin (Mueller et al., 2012) or at the home source from single frozen crystals. The structures were solved by MR-SAD and MR techniques, and further refined as described in detail in the Supplemental Information.

In Vitro Pull-Downs

Ni-NTA Sepharose beads (Macherey-Nagel) were mixed with an N-terminally His₆GB1-tagged 3A protein at a final concentration of 100 μM and an untagged ACBD3 protein (wild-type or mutant as indicated) at a final concentration of 30 μM in the binding buffer (30 mM Tris [pH 8], 200 mM NaCl, 10 mM imidazole, and 3 mM β -mercaptoethanol). After 60 min incubation at 4°C the beads were washed three times with the binding buffer and the total protein was directly eluted with the Laemmli sample buffer and analyzed by SDS-PAGE.

Analytical Ultracentrifugation

Sedimentation velocity experiments were performed using a ProteomeLab XL-I Beckman Coulter analytical ultracentrifuge equipped with an An-50 Ti rotor. All measurements were conducted in the size-exclusion chromatography (SEC) buffer at 20°C and 42,000 rpm. All data were collected using the absorbance (280 nm) optical system and analyzed using a sedimentation coefficient distribution model c(s).

SPR

SPR measurements were performed on a four-channel SPR sensor platform (Plasmon IV) developed at the Institute of Photonics and Electronics, AS CR, as described previously (Klima et al., 2016) and as described in detail in Supplemental Information.

MST

MST measurements were performed using the Monolith NT.115 instrument and the Monolith NT.115 standard treated capillaries (NanoTemper Technologies) according to the manufacturer's instructions. The capillaries were loaded with a mixture of a recombinant EGFP-fused protein at a constant concentration of 100 nM in the SEC buffer and its binding partner in the indicated series of concentrations. The changes in thermophoresis were analyzed with the Monolith NT Analysis Software.

Large Unilamellar Vesicles Preparation and Fluorescence Correlation Spectroscopy

Large unilamellar vesicles (LUVs) composed of 1-palmitoyl 2-oleoyl-phosphatidylcholine (POPC) (54.99 mol %), 1-palmitoyl-2-oleoyl-*sn*-glycero-3-phosphoserine (POPS) (20 mol %), cholesterol (20 mol %), DGS-NTA(Ni) (5 mol %) (Avanti Polar Lipids), and ATTO647N-DOPE (0.01 mol %) (ATTO-TEC) were prepared from the appropriate chloroform mixture. The chloroform was evaporated; the lipid film was dried in vacuum and re-hydrated with the LUV buffer (10 mM Tris [pH 7.4], 10 mM MgCl₂, 20 mM imidazol, and 150 mM NaCl). The turbid solution containing multilamellar vesicles was extruded 21 times with use of 100-nm filters in an AVESTIN extruder (AVESTIN). LUVs were mixed with the recombinant EGFP-fused GOLD domain (wild-type or LW mutant as indicated) at a final concentration of 20 nM and the His₆-3A-His₆ protein at a final concentration ranging from 0 to 16 μM in the LUV buffer, and then were subjected to fluorescence correlation spectroscopy (FCS) experiment as detailed in Supplemental Information.

Giant Unilamellar Vesicles Preparation and Imaging

Giant unilamellar vesicles (GUVs) composed of POPC (55 mol %), POPS (5 mol %), PI4P (5 mol %), cholesterol (20 mol %), PI (10 mol %), and DGS-NTA(Ni) (5 mol %) were prepared by electroformation. The lipid mixture dissolved in chloroform was spread on each electrode (5 × 5 cm indium tin oxide-coated glass) and dried in vacuum. The lipid-coated electrodes were incubated in a homemade Teflon chamber with 600 mM sucrose, while an altering current with a maximum voltage amplitude of 1 V and a frequency of 10 Hz was applied for 1 hr. The images of GUVs were taken on the laser scanning microscope LSM780 (Zeiss). To avoid crosstalk, CFP and GFP were excited separately. CFP and GFP were excited with the 405 and 488 nm laser lines, respectively, and the emissions were collected between 490 and 595 nm.

Molecular Modeling and MD Simulations

The atomic coordinates of the GOLD:3A complex were taken from the crystal structure reported in this study. The intrinsically disordered loop of the GOLD domain missing in the crystal structure (i.e., residues T436-K473) was modeled using MODELLER (Fiser et al., 2000). The C-terminal segment of the 3A protein missing in the crystal structure (i.e., residues G35-T90) was introduced as follows: The segment I40-P78 was modeled using SWISS MODEL (Biasini et al., 2014); the residues G35-I40 and R81-T90 were modeled using MODELLER; the predicted transmembrane region of the 3A protein, involving residues I60-A80, was positioned in the membrane environment using the PPM server (Lomize et al., 2006).

The initial system for MD simulations was prepared using VMD version 1.9.2 (Humphrey et al., 1996). Namely, a POPC bilayer segment with the lateral dimensions of 10 × 10 nm was formed using the Membrane Plugin version 1.1

in VMD. The full-length GOLD:3A complex was placed on top of the resulting lipid patch. The lipids overlapping with the transmembrane α helix or the myristoylated G1 residue of 3A were removed. The system was solvated using the Solvate Plugin version 1.5 in VMD. Sodium and chloride ions were added to neutralize the simulated system and to reach a physiological ion concentration of 150 mM. The MD simulations were performed using NAMD 2.9 (Phillips et al., 2005) as detailed in Supplemental Information.

ACCESSION NUMBERS

The accession numbers for the crystal structures of the unliganded human ACBD3 GOLD domain, the GOLD domain in complex with the 3A protein of *Aichivirus A*, and the GOLD domain in complex with the 3A protein of *Aichivirus B* reported in this paper are PDB: 5LZ1, 5LZ3, and 5LZ6, respectively.

SUPPLEMENTAL INFORMATION

Supplemental Information includes Supplemental Experimental Procedures, two figures, two tables, one movie, and three 3D molecular models and can be found with this article online at <http://dx.doi.org/10.1016/j.str.2016.11.021>.

AUTHOR CONTRIBUTIONS

M.K. designed and performed most of the experiments, analyzed the data, and wrote the manuscript, D.C. contributed to the DNA cloning, protein purifications, and MST measurements, B.R. performed the molecular modeling and molecular dynamics simulations, J.H. carried out the LUVs preparation and the FCS experiment, L.R. performed the analytical ultracentrifugation experiment, J.S., A.B., and A.D. contributed to protein purifications, E.B. carried out the GUVs preparation and imaging, supervised the project, and revised the manuscript.

ACKNOWLEDGMENTS

We are grateful to Prof. Carolyn Machamer (Johns Hopkins University, Baltimore, MD) for sharing the ACBD3 encoding plasmid, Prof. Joseph DeRisi (UCSF School of Medicine, San Francisco, CA) for sharing the synthetic Aichivirus genome, Jaroslav Srp (IOCB, Prague, Czech Republic) for a technical help with microscale thermophoresis. We thank Helmholtz-Zentrum Berlin for the allocation of synchrotron radiation beamtime. We are grateful to Tamas Balla for critical reading of the manuscript and for fruitful discussions. The work was supported by the Czech Science Foundation (grant 17-07058Y) and by the Academy of Sciences of the Czech Republic (RVO: 61388963).

Received: October 11, 2016

Revised: November 8, 2016

Accepted: November 28, 2016

Published: January 5, 2017

REFERENCES

- Anantharaman, V., and Aravind, L. (2002). The GOLD domain, a novel protein module involved in Golgi function and secretion. *Genome Biol.* 3, research0023.
- Biasini, M., Bienert, S., Waterhouse, A., Arnold, K., Studer, G., Schmidt, T., Kiefer, F., Gallo Cassarino, T., Bertoni, M., Bordoli, L., et al. (2014). SWISS-MODEL: modelling protein tertiary and quaternary structure using evolutionary information. *Nucleic Acids Res.* 42, W252–W258.
- Deitz, S.B., Dodd, D.A., Cooper, S., Parham, P., and Kirkegaard, K. (2000). MHC I-dependent antigen presentation is inhibited by poliovirus protein 3A. *Proc. Natl. Acad. Sci. USA* 97, 13790–13795.
- Dodd, D.A., Giddings, T.H., and Kirkegaard, K. (2001). Poliovirus 3A protein limits interleukin-6 (IL-6), IL-8, and beta interferon secretion during viral infection. *J. Virol.* 75, 8158–8165.
- Dorobantu, C.M., van der Schaar, H.M., Ford, L.A., Strating, J.R.P.M., Ulferts, R., Fang, Y., Belov, G., and van Kuppeveld, F.J.M. (2014). Recruitment of P14KIIIβ to coxsackievirus B3 replication organelles is independent of ACBD3, GBF1, and Arf1. *J. Virol.* 88, 2725–2736.

- Dorobantu, C.M., Albulescu, L., Harak, C., Feng, Q., van Kampen, M., Strating, J.R.P.M., Gorbalenya, A.E., Lohmann, V., van der Schaar, H.M., and van Kuppeveld, F.J.M. (2015a). Modulation of the host lipid landscape to promote RNA virus replication: the picornavirus encephalomyocarditis virus converges on the pathway used by hepatitis C virus. *PLoS Pathog.* *11*, e1005185.
- Dorobantu, C.M., Ford-Siltz, L.A., Sittig, S.P., Lanke, K.H.W., Belov, G.A., van Kuppeveld, F.J.M., and van der Schaar, H.M. (2015b). GBF1- and ACBD3-independent recruitment of PI4KIII β to replication sites by rhinovirus 3A proteins. *J. Virol.* *89*, 1913–1918.
- Fan, J., Liu, J., Culty, M., and Papadopoulos, V. (2010). Acyl-coenzyme A binding domain containing 3 (ACBD3; PAP7; GCP60): an emerging signaling molecule. *Prog. Lipid Res.* *49*, 218–234.
- Fiser, A., Do, R.K., and Sali, A. (2000). Modeling of loops in protein structures. *Protein Sci.* *9*, 1753–1773.
- Fujita, K., Krishnakumar, S.S., Franco, D., Paul, A.V., London, E., and Wimmer, E. (2007). Membrane topography of the hydrophobic anchor sequence of poliovirus 3A and 3AB proteins and the functional effect of 3A/3AB membrane association upon RNA replication. *Biochemistry* *46*, 5185–5199.
- Greninger, A.L., Knudsen, G.M., Betegon, M., Burlingame, A.L., and Derisi, J.L. (2012). The 3A protein from multiple picornaviruses utilizes the Golgi adaptor protein ACBD3 to recruit PI4KIII β . *J. Virol.* *86*, 3605–3616.
- Greninger, A.L., Knudsen, G.M., Betegon, M., Burlingame, A.L., and Derisi, J.L. (2013). ACBD3 interaction with TBC1 domain 22 protein is differentially affected by enteroviral and kobuviral 3A protein binding. *MBio* *4*, e00098–e00113.
- Hsu, N.-Y., Ilnytska, O., Belov, G., Santiana, M., Chen, Y.-H., Takvorian, P.M., Pau, C., van der Schaar, H., Kaushik-Basu, N., Balla, T., et al. (2010). Viral reorganization of the secretory pathway generates distinct organelles for RNA replication. *Cell* *141*, 799–811.
- Humphrey, W., Dalke, A., and Schulten, K. (1996). VMD: visual molecular dynamics. *J. Mol. Graph.* *14*, 33–38, 27–8.
- Ishikawa-Sasaki, K., Sasaki, J., and Taniguchi, K. (2014). A complex comprising phosphatidylinositol 4-kinase III β , ACBD3, and Aichi virus proteins enhances phosphatidylinositol 4-phosphate synthesis and is critical for formation of the viral replication complex. *J. Virol.* *88*, 6586–6598.
- Klima, M., Toth, D.J., Hexnerova, R., Baumlova, A., Chalupska, D., Tykvar, J., Rezabkova, L., Sengupta, N., Man, P., Dubankova, A., et al. (2016). Structural insights and in vitro reconstitution of membrane targeting and activation of human PI4KB by the ACBD3 protein. *Sci. Rep.* *6*, 23641.
- Lomize, M.A., Lomize, A.L., Pogozheva, I.D., and Mosberg, H.I. (2006). OPM: orientations of proteins in membranes database. *Bioinformatics* *22*, 623–625.
- Mueller, U., Darowski, N., Fuchs, M.R., Förster, R., Hellmig, M., Paithankar, K.S., Pühringer, S., Steffien, M., Zocher, G., and Weiss, M.S. (2012). Facilities for macromolecular crystallography at the Helmholtz-Zentrum Berlin. *J. Synchrotron Radiat.* *19*, 442–449.
- Phillips, J.C., Braun, R., Wang, W., Gumbart, J., Tajkhorshid, E., Villa, E., Chipot, C., Skeel, R.D., Kalé, L., and Schulten, K. (2005). Scalable molecular dynamics with NAMD. *J. Comput. Chem.* *26*, 1781–1802.
- Reuter, G., Boros, Á., and Pankovics, P. (2011). Kobuviruses – a comprehensive review. *Rev. Med. Virol.* *21*, 32–41.
- Sabin, C., Füzik, T., Škubník, K., Pálková, L., Lindberg, A.M., and Plevka, P. (2016). Structure of Aichi virus 1 and its empty particle: clues towards kobuvirus genome release mechanism. *J. Virol.* <http://dx.doi.org/10.1128/JVI.01601-16>.
- Sasaki, J., Ishikawa, K., Arita, M., and Taniguchi, K. (2012). ACBD3-mediated recruitment of PI4KB to picornavirus RNA replication sites. *EMBO J.* *31*, 754–766.
- Schwille, P., Meyer-Almes, F.J., and Rigler, R. (1997). Dual-color fluorescence cross-correlation spectroscopy for multicomponent diffusional analysis in solution. *Biophys. J.* *72*, 1878–1886.
- Sohda, M., Misumi, Y., Yamamoto, A., Yano, A., Nakamura, N., and Ikehara, Y. (2001). Identification and characterization of a novel Golgi protein, GCP60, that interacts with the integral membrane protein giantin. *J. Biol. Chem.* *276*, 45298–45306.
- Strauss, D.M., Glustrom, L.W., and Wuttke, D.S. (2003). Towards an understanding of the poliovirus replication complex: the solution structure of the soluble domain of the poliovirus 3A protein. *J. Mol. Biol.* *330*, 225–234.
- Wessels, E., Duijsings, D., Niu, T.-K., Neumann, S., Oorschot, V.M., de Lange, F., Lanke, K.H.W., Klumperman, J., Henke, A., Jackson, C.L., et al. (2006). A viral protein that blocks Arf1-mediated COP-I assembly by inhibiting the guanine nucleotide exchange factor GBF1. *Dev. Cell* *11*, 191–201.
- Yang, J., Yan, R., Roy, A., Xu, D., Poisson, J., and Zhang, Y. (2014). The I-TASSER Suite: protein structure and function prediction. *Nat. Methods* *12*, 7–8.
- Zhu, L., Wang, X., Ren, J., Kotecha, A., Walter, T.S., Yuan, S., Yamashita, T., Tuthill, T.J., Fry, E.E., Rao, Z., et al. (2016). Structure of human Aichi virus and implications for receptor binding. *Nat. Microbiol.* *1*, 16150.